Role of convection in microstructure evolution during solidification

Anirban Bhattacharya and Pradip Dutta*

Department of Mechanical Engineering, Indian Institute of Science, Bangalore 560 012, India

In this study, we present a new computational approach for studying the effect of melt convection on solidification at the micro-scale level. Models for dendritic and eutectic growth are developed on the basis of the enthalpy technique and incorporate the presence of flow in the domain. Simulation results show the growth and motion of dendrites and evolution of eutectic lamellae and their interaction with melt flow. The present study provides the foundation for development of an efficient generalized micro-scale solidification model, which can potentially be coupled with system-scale models based on the same framework.

Keywords: Convection, dendrite growth, enthalpy method, eutectic, micro-scale solidification.

SOLIDIFICATION is a fundamental phenomenon which is encountered in almost every aspect of life – from simple household affairs such as formation of ice in the freezer, to complex industrial applications, a range of manufacturing processes, and even large-scale natural events. It follows that a thorough understanding of the mechanisms of solidification is essential for many important fields such as industrial manufacturing and applications, biology, medicine, micro and nano-technology, and geological and climate studies. From a manufacturing point of view, one of the most important applications of solidification is the prediction of microstructure formation during a casting process.

Casting can be used economically for obtaining products with desired shape and properties and can handle a large range of sizes and complexities. The properties of a cast product such as its strength, toughness and so forth, depend on its microstructure. By controlling the formation of microstructure during solidification, a cast product can be made to attain required properties. Hence, the study of microstructure evolution and its interaction with various phenomena associated with solidification assumes great importance.

To understand the different aspects of solidification, let us consider a typical casting process for an alloy as shown schematically in Figure 1. We can observe that solidification progresses from the mould walls towards the interior due to heat transfer from the walls. At the system-scale, three regions can be differentiated in the solidifying alloy. Adjacent to the mould walls is a completely solidified zone, while the innermost zone contains only liquid metal. In between these two regions, there is a third zone where both the liquid and solid co-exist. This region, known as the mushy zone, is of particular importance as several significant phenomena related to solidification occur in this zone. We can also observe that there are large convection cells at the system-scale level developing due to the presence of thermal gradients. In addition, as the solubility of the solute in solid is usually less than that in liquid, solute segregation (or partitioning) occurs at the solid–liquid interface, leading to a solutal (or concentration) gradient. This concentration gradient causes solutally driven convection at the local as well as system-scale. The interaction of thermo-solutal convection with the mushy zone affects the solidification process and as a result the final microstructure.

To understand this further, we have to study the mushy region at the microscopic scale. As we can observe from Figure 1, solidification proceeds with an unstable interface through the formation of branched tree-like structures known as dendrites. The dendrites which grow into the melt from the solid with a directional preference are known as columnar dendrites while those evolving in the melt without any directional preference are known as equiaxed dendrites. Melt flow is present in this region due to system-scale thermo-solutal convection. Additionally, at the solid–liquid interface, occurrence of solidification leads to shrinkage as the density of solid is usually greater than that of liquid. This shrinkage at the solidification interface causes convection towards the interface. Equiaxed dendrites can move freely as a result of this thermo-solutal and shrinkage-driven convection. They can also be stationary if the solid fraction becomes higher than a critical value. In both cases, their interaction with the melt flow significantly affects their growth pattern.

Another important aspect of solidification is the formation of eutectic microstructure which occurs when the solute concentration at any region reaches the eutectic composition. Eutectic solidification is characterized by the simultaneous evolution of two different solid phases from the melt. The presence of alternate layers of solute enrichment and solute depletion adjacent to the solidification front leads to micro-scale convection in that region affecting the eutectic growth pattern. Casting defects such as shrinkage voids and gas porosity are also formed in the mushy zone. Shrinkage voids occur when a region gets cut off from the melt, and liquid in-flow cannot compensate for the change in volume. Gas porosity occurs when a gas bubble gets trapped in the solidifying front or in between dendrite branches. All these phenomena interact with each other and contribute towards the final morphology of the cast product.

Over the last three decades, significant effort has been directed towards computational study of solidification. Numerical models have been developed for better understanding of the factors governing the process of solidification. Most of the initial models[1–6] simulate pure metal

*For correspondence. (e-mail: pradip@mecheng.iisc.ernet.in)

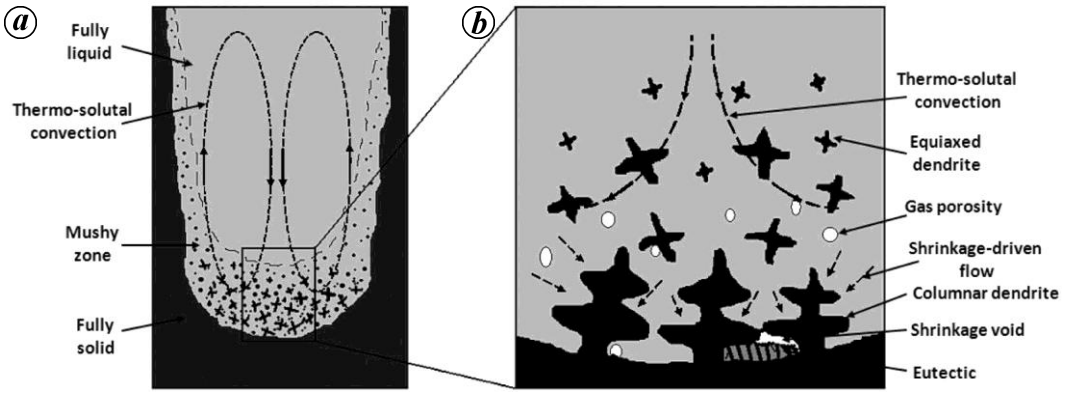

Figure 1. Schematic diagram showing various system-scale and micro-scale phenomena occurring during a typical casting process.

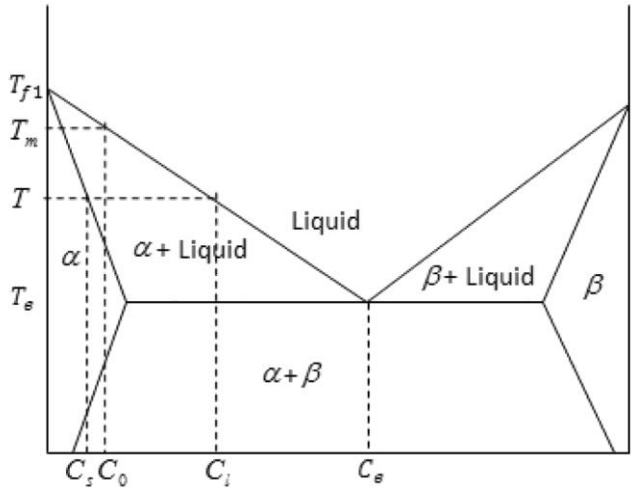

Figure 2. Representative phase diagram for a binary alloy.

or alloy solidification at the system-scale level treating the mushy region for alloys as a porous medium with calculated average properties. Though these models are unable to resolve the actual details of the solidifying front in the mushy zone, they nevertheless provide important insight towards system-scale phenomena such as macro-scale segregation of solute in the casting, formation and characteristics of convection cells, and influence of the boundary conditions on the growth rate and pattern.

In recent years, numerical models have also been developed for studying solidification directly at the microscopic scale. These models simulate the various micro-scale forms of solidification such as the growth of equiaxed or columnar dendrites[7–10], eutectic growth and formation of complex eutectic microstructure[11–13]. These models are useful for understanding microstructure formation patterns and their dependence on local thermo-solutal distribution. The presence of complex interface shapes and the necessity of accurate curvature calculation present significant challenges for developing such models. Convection generates an additional level of complexity, and hence, relatively fewer models[14–17] are available in the literature which incorporates the effect of melt convection on the growth morphology.

In this study, we present computational models for studying the effect of melt flow on (a) Growth of stationary equiaxed dendrites, (b) Simultaneous growth and movement of free equiaxed dendrites and (c) Evolution of eutectic microstructure. The models are developed based on the popular enthalpy method for solidification[3,5] and follows the same generalized numerical framework. The volume of fluid (VOF) method[18] is implemented to track the movement of dendrites. For simulating eutectic solidification, the enthalpy method has been modified to incorporate the coexistence of the two solid phases and the presence of triple-phase equilibrium point. A detailed description of the modelling procedure and the associated numerical intricacies follows.

Figure 2 shows a typical linearized phase diagram denoting the presence of various phases and their equilibrium temperature and concentration. During a casting process, solidification starts corresponding to the liquid zone in the phase diagram. For example, the initial melt may have a concentration of C_0 with a melting temperature T_m. As temperature decreases, solidification progresses and α phase is generated in the melt. Due to reduced concentration of solute in the α phase, solute gets rejected into the liquid. This is known as solute partitioning and results in the accumulation of solute ahead of the interface and hence increasing the local concentration value in the liquid. When the solute concentration reaches the eutectic value, C_e, both α and β phases are simultaneously generated. We should note that during the entire process, the temperature–concentration relation as governed by the phase diagram is always satisfied. For developing a numerical model for solidification, the energy and solute transport equations need to be solved taking into account the temperature–concentration coupling according to the phase diagram. Additionally, for simulating the melt flow, the continuity and momentum equations also need to be solved.

Conservation equations for the entire computational domain are derived by volume averaging the individual phase equations as given by Bennon and Incropera[1,2]. For that purpose, the equivalent mixture density and velocity are defined as $\rho = \sum_k \rho_k g_k$ and $\vec{u} = \sum_k \vec{u}_k f_k$, where g_k is the volume fraction and f_k is the mass fraction of phase k. Such an averaging approach, together with the assumption of constant phase densities, leads to the equivalent single-phase governing equation as stated below in their non-dimensional forms.

The energy equations is defined as

$$\frac{\partial}{\partial t^*}(h^*) + \nabla^* \cdot (\vec{u}^* h^*) = \nabla^* \cdot (K^* \nabla^* T^*). \quad (1)$$

The solute transport equation is defined as

$$\frac{\partial}{\partial t^*}(C^*) + \nabla^* \cdot (\vec{u}^* q^*) = \nabla^* \cdot (D^* \nabla^* q^*). \quad (2)$$

The continuity and momentum equations are written as

$$\nabla^* \cdot (\vec{u}^*) = 0, \quad (3)$$

$$\frac{\partial}{\partial t^*}(\vec{u}^*) + \nabla^* \cdot (\vec{u}^* \vec{u}^*) = \nabla^* \cdot (\mathrm{Pr} \nabla^* \vec{u}^*) - \nabla^* p^*. \quad (4)$$

In eqs (1)–(4), h^*, T^*, K^*, C^* and D^* are respectively the dimensionless enthalpy, temperature, volume averaged conductivity, solute concentration and the modified solute diffusivity. $\vec{u}^*$ is the dimensionless velocity, p^* is the dimensionless pressure and Pr denotes the Prandtl number of the fluid. These four equations together with the definition of interface temperature and the temperature–solute coupling as per the phase diagram form the basis of both the dendrite growth and the eutectic models. The use of average enthalpy value at each computational node to calculate the position of solidification interface characterizes the enthalpy method used in these models. The following sub-sections highlight the differences between the dendrite growth and eutectic growth models.

For the dendrite growth model, the dimensionless enthalpy h^* is defined as

$$h^* = \frac{T - T_\mathrm{f} - mC_0}{L/c} + f_\mathrm{l},$$

while the concentration potential q^* is defined as

$$q^* = \frac{C^*}{k_p + (1 - k_p) f_l}$$

where L, c, k_p and m are the latent heat of solidification, specific heat, partition coefficient and slope of the liquidus line, respectively. The concentration potential acts as a pseudo-liquid concentration value which can be applied to the solid phases[10]. The actual temperature at the solidification interface is different from the prescribed melting temperature because of the presence of surface tension and due to solute accumulation at the interface. Taking these effects into account, the non-dimensional interface temperature is given by

$$T_i^* = -\kappa^* d(\theta)/d_0 + MC_0(1 - q^*). \quad (5)$$

In eq. (5), the first term $-\kappa^* d(\theta)/d_0$ is known as curvature undercooling and accounts for the surface tension effects. The term $d(\theta) = \gamma(\theta) T_\mathrm{m} c/L^2$ is anisotropic capillary length, κ^* is curvature and d_0 is the length scale. The term $MC_0(1 - q^*)$ represents the solutal under-cooling, where C_0 is the initial concentration and M is the slope of the liquidus line in non-dimensional form. The anisotropy in dendrite growth is accounted for by using the model $d(\theta) = d_0(1 - 15\varepsilon \cos 4\theta)$, where ε and θ are the anisotropy strength and interface angle respectively. The curvature of the interface is calculated using a level set technique[19] as given by Voller[10].

Simulation of eutectic growth presents further challenges due to the higher number of phases and additional complexities associated with triple junction equilibrium. To incorporate the presence of two solid phases, a beta phase fraction parameter g_β is defined where g_β is the volume fraction of beta phase in solid. Using f_l and g_β, the definitions of the averaged specific enthalpy h^* and concentration C^* are modified as

$$h^* = \left(f_\mathrm{l} + (1 - f_\mathrm{l}) \left(\frac{c_\alpha}{c_\mathrm{l}} (1 - g_\beta) + \frac{c_\beta}{c_\mathrm{l}} g_\beta \right) \right) T^* - \left(1 - f_\mathrm{l}\right) \left((1 - g_\beta) + \frac{L_\beta}{L_\alpha} g_\beta \right)$$

and

$$C^* = f_\mathrm{l} C_\mathrm{l} + (1 - f_\mathrm{l})((1 - g_\beta) C_\alpha + g_\beta C_\beta).$$

Subscripts l, α and β denote liquid, alpha and beta phases respectively. Enthalpy is calculated by considering the melt at eutectic temperature as the reference state. Concentration potential q^* is defined as

$$q^* = \frac{C^* - (1 - f_\mathrm{l}) g_\beta (1 - k_\beta)}{f_\mathrm{l} + (1 - f_\mathrm{l})((1 - g_\beta) k_\alpha + g_\beta k_\beta)}.$$

Interface temperature is modified appropriately to account for the presence of the two solid phases.

The movement of dendrites is simulated using VOF method[18]. The flow field obtained by solving the mass

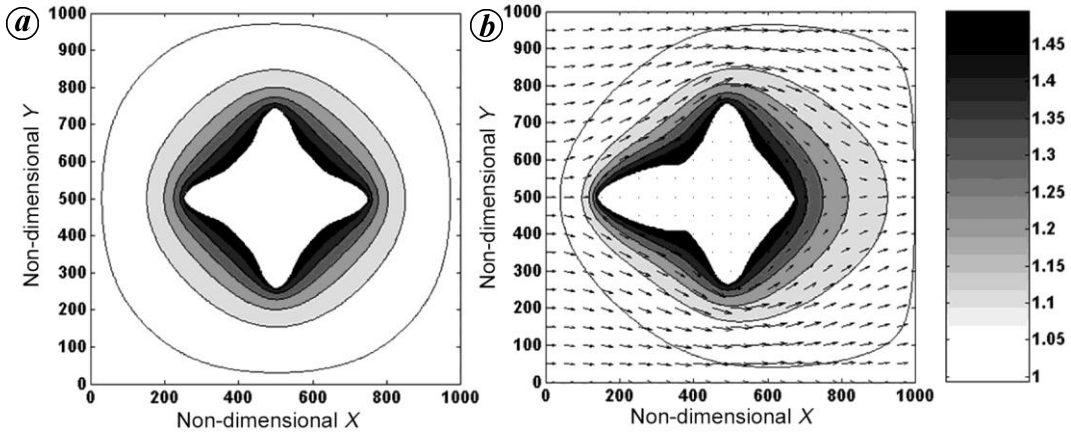

Figure 3. Comparison of dendrite shape and concentration contours at non-dimensional time t = 20,000. (***a***) Without flow and (***b***) with dimensionless flow velocity of u = 0.02.

and momentum conservation equations governs the motion of the dendrites. In the VOF method, liquid fraction field f_1 is advected while preserving its shape and conserving its mass. This movement is governed by the equation

$$\frac{\partial f_1}{\partial t^*} + \vec{u}^* \cdot \nabla^* (f_1) = 0. \quad (6)$$

Further details of the implementation technique for the VOF model used here is present in Gerlach *et al.*[20].

The governing equations are solved in a Cartesian co-ordinate system using a two-dimensional rectangular computational domain, which is uniformly divided into square control-volumes. For obtaining the velocity field, staggered grids are employed. Initially, the domain is completely occupied by liquid at an under-cooled temperature T_u. When melt flow is present, uniform inflow and outflow velocities are specified at the required faces, and symmetry conditions are imposed on the other faces. The growth of the solid phases is initiated by the introduction of seed crystals. The algorithm for each time step can be briefly described as follows.

1. Solve the energy and solute transport equations using the explicit finite difference method described by Voller[10] to obtain the enthalpy and solute concentration at each node. The velocity field from the previous time step is used for solving these equations.
2. Calculate interface curvature and interface temperature.
3. Using the interface temperature and the temperature–concentration relation from the phase diagram, calculate the temperature, concentration potential and the phase fraction parameters for the entire domain.
4. If dendrite movement is allowed, solve the VOF advection equation and reconstruct the interface using the LVIRA technique[20].
5. Solve the mass and momentum conservation equations using the SIMPLER algorithm[21] and a TDMA (Tri-Diagonal Matrix Algorithm) solver to obtain the updated velocity field.

Here, we first present the simulation results for the effect of convection on stationary dendrites. This is followed by results for simultaneous growth and motion of dendrites. Finally, results for eutectic growth are presented.

When an external melt flow is imposed in the micro-scale domain, the shape of a growing dendrite is governed by the flow direction and velocity. Such an external forced flow can act as representative of the thermo-solutal convection occurring at the system-scale level. To observe the effect of this type of flow on dendrite morphology, simulations were performed for equiaxed dendrite growth with and without convection. Figure 3 shows a comparison for the growth pattern and the solute concentration fields for the two cases. For the simulations, an undercooling of $T_u = -0.5$ was used. The size of the domain is 1000×1000, while a grid size of $\Delta x = 2.5$ and time step of $\Delta t = 0.5$ were used. The dendrite shapes were plotted at a time t = 20,000. A flow velocity of $u = 0.02$ was introduced from the left side of the domain for the second case. All the given values are in non-dimensional form. Grid independence was established and it was found that grid sizes smaller than $\Delta x = 2.5$ give almost identical results.

From Figure 3 *a*, it is observed in the absence of melt convection, the dendrite arms grow symmetrically in the four directions. Due to partitioning, solute accumulation occurs adjacent to the interface, which is slowly diffused away into the melt. When melt convection is present, the dendrite arms grow asymmetrically along the flow direction (Figure 3 *b*). This is because in presence of flow, higher heat transfer and solute transport occur on the upstream side of the dendrite resulting in higher growth rate. Additionally, convection current removes accumu-

lated solute from the upstream side which increases the interface temperature. This causes higher temperature gradient at the solid–liquid interface resulting in further increase of the growth rate. The downstream arm grows slower due to the velocity shading effect of the side arms leading to higher solute accumulation and inefficient heat transfer at the interface. Convection of solute from the upstream side and the resulting non-uniform concentration field can be clearly observed in Figure 3 *b*.

To observe the interaction of multiple dendrites growing in a convecting melt, we introduced five seed crystals in a domain of size 2000×2000 with an undercooled melt at a temperature of $T_u = -0.6$. External convection was imposed using a velocity of $u = 0.05$ from the lower boundary. All the dendrites were oriented at an angle of 45° to the horizontal by suitably modifying the anisotropy term in the curvature undercooling.

Figure 4 *a* and *b* show the dendrite growth pattern and concentration contours at time $t = 6000$ and $t = 20{,}000$ respectively. It can be observed from Figure 4 *a*, that similar to the single dendrite in Figure 3, the arms in the upstream directions grow at a higher rate. All the dendrite shapes are similar and concentration fields surrounding them do not significantly interact with each other. When the dendrites grow larger, as observed in Figure 4 *b*, the solute concentration fields start to interact with each other. As a result of higher solute accumulation at the central region, the growth of the central dendrite is stunted. For the other dendrites, the arms facing the central region grow slowly while the free arms are characterized by efficient solute removal due to convection leading to a higher growth rate.

During a casting process, equiaxed dendrites which are away from the interface can freely move in the melt as a result of convection. To study such a situation, simultaneous growth and motion of a dendrite was simulated in a domain of size 2000×1000. An undercooling $T_u = -0.25$ and flow velocity of $u = 0.005$ were used. Figure 5 shows the variation of dendrite shape and position with time. The initial and final positions (corresponding to time $t = 3000$ and $t = 195{,}000$ respectively) are shown by the solid contours while the intermediate shapes are shown using dotted lines. It can be observed that, in this case, though the upstream arm grows at a higher rate, the asymmetry of the dendrite arms is significantly less than for those shown in Figure 3. The growth reduction in the downstream arm is not as extreme because of the absence of relative motion between the dendrite arm and the melt. This type of simultaneous growth and motion can result in interesting scenarios because of the competing nature of the growth velocity and convection velocity.

To simulate eutectic growth, we consider the evolution of alpha and beta phase lamellae from a melt of eutectic composition held at the eutectic temperature. A constant cooling condition is specified at the lower boundary while zero flux condition is imposed on the other boundaries. Seeds for alpha and beta phases are placed alternately at the bottom wall of the domain. A symmetric phase diagram is considered with an eutectic composition of $C_e = 0.05$. Initial alpha and beta concentrations are

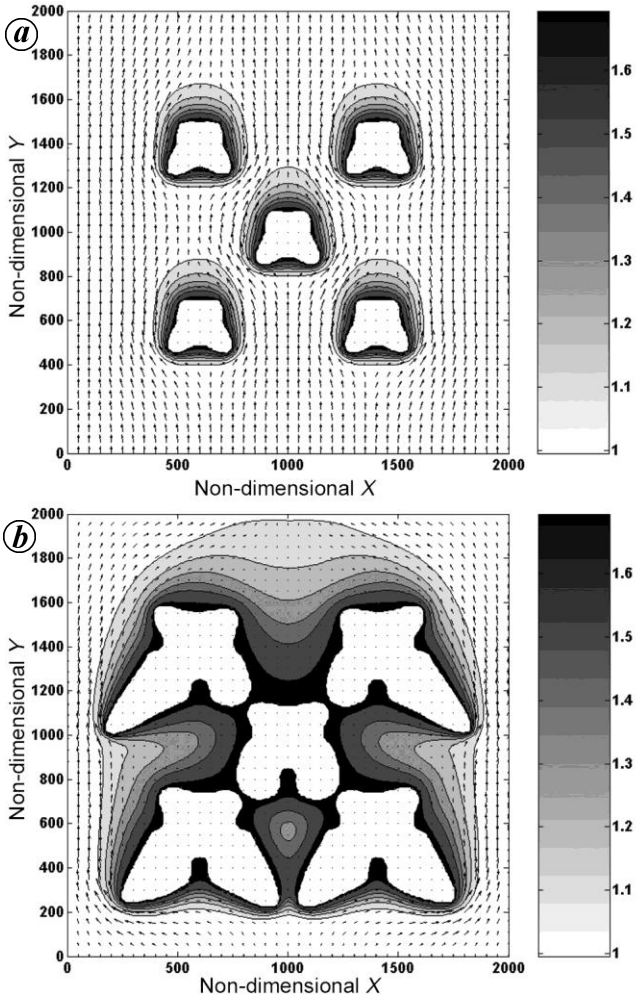

Figure 4. Growth pattern, concentration contours and velocity vectors for multiple dendrites evolving in a convecting melt. ***a***, At non-dimensional time $t = 6000$; ***b***, at $t = 20{,}000$.

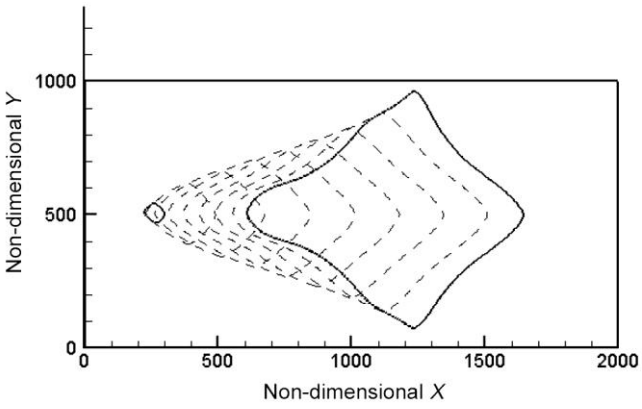

Figure 5. Growth and movement of dendrite in a convecting melt with $u = 0.005$.

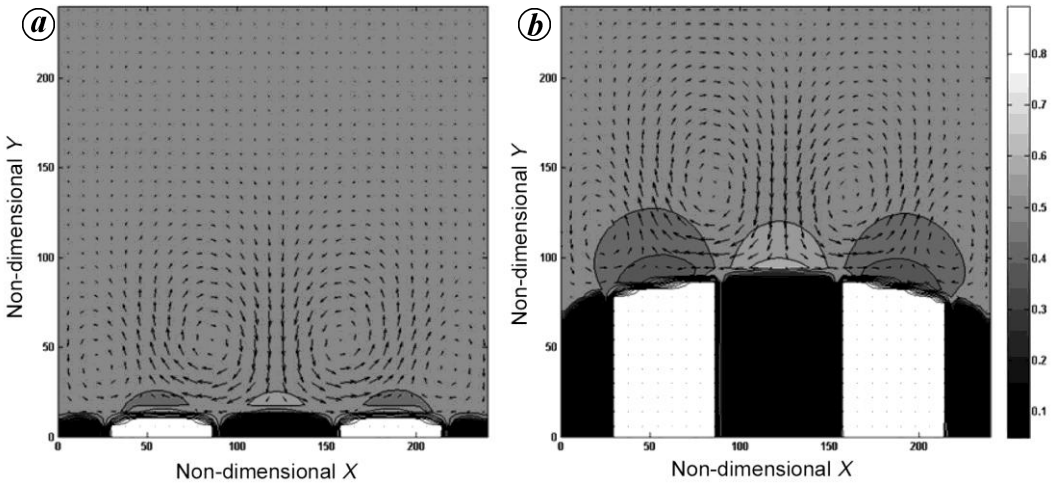

Figure 6. Eutectic front position, velocity vectors and concentration contours: ***a***, At t = 4000; ***b***, at t = 32,000.

C_α = 0.05 and C_β = 0.95 respectively. Convection occurs in the domain due to establishment of solute gradients in the liquid resulting in solutal buoyancy effects. This is simulated using the Boussinesq approximation.

Figure 6 *a* and *b* show the growth pattern of the eutectic phases and the associated concentration profile at time t = 4000 and t = 32,000 respectively. The expected concentration profile is observed with solute accumulation in front of the alpha phase and depletion in front of the beta phase lamellae. It can be seen that rejection of the heavier solute in front of the alpha phase lamella causes the liquid to move downwards whereas the opposite occurs in front of the beta phase lamella. This gives rise to flow cells ahead of the eutectic interface causing enhanced solute transfer between the two phases.

A new approach is presented to model the growth of dendritic and eutectic microstructure and their interaction with melt convection. The developed models are useful for studying complex microstructure formation and its dependence on important flow parameters governing the solidification process. The models can be extended to develop a generalized microstructure evolution model.

1. Bennon, W. D. and Incropera, F. P., A continuum model for momentum, heat and species transport in binary solid–liquid phase change system-I. Model formulation. *Int. J. Heat Mass Transf.*, 1987, **30**, 2161–2170.
2. Bennon, W. D. and Incropera, F. P., A continuum model for momentum, heat and species transport in binary solid–liquid phase change system-II. Application to solidification in a rectangular cavity. *Int. J. Heat Mass Transf.*, 1987, **30**, 2171–2187.
3. Brent, A. D., Voller, V. R. and Reid, K. J., Enthalpy–Porosity technique for modeling convection–diffusion phase change: Application to the melting of a pure metal. *Numer. Heat Transf., Part A. Applications*, 1988, **13**, 297–318.
4. Voller, V. R., Brent, A. D. and Prakash, C., The modelling of heat, mass and solute transport in solidification systems. *Int. J. Heat Mass Transf.*, 1989, **32**, 1719–1731.
5. Chakraborty, S. and Dutta, P., A generalized formulation for evaluation of latent heat functions in enthalpy-based macroscopic models for convection–diffusion phase change processes. *Metall. Mater. Trans. B*, 2001, **32**, 562–564.
6. Chakraborty, S. and Dutta, P., The effect of solutal undercooling on double-diffusive convection and macrosegregation during binary alloy solidification: a numerical investigation. *Int. J. Numer. Meth. Fluids*, 2002, **38**, 895–917.
7. Kobayashi, R., Modeling and numerical simulations of dendritic crystal growth. *Physica D*, 1993, **63**, 410–423.
8. Karma, A. and Rappel, W., Quantitative phase field modeling of dendritic growth in two and three dimensions. *Phys. Rev. E*, 1998, **57**, 4323–4349.
9. Gandin, A. and Rappaz, M., A 3d cellular automaton algorithm for the prediction of dendritic grain growth. *Acta Mater.*, 1997, **45**, 2187–2195.
10. Voller, V. R., An enthalpy method for modeling dendritic growth in a binary alloy. *Int. J. Heat Mass Transf.*, 2008, **51**, 823–834.
11. Karma, A., Phase-field model of eutectic growth. *Phys. Rev. E*, 1994, **49**, 2245–2250.
12. Wheeler, A. A., McFadden, G. B. and Boettinger, W. J., Phase-field model for solidification of a eutectic alloy. *Proc. R. Soc. Lond. Series A: Math., Phys. Eng. Sci.*, 1996, **452**, 495–525.
13. Folch, R. and Plapp, M., Quantitative phase-field modeling of two-phase growth. *Phys. Rev. E*, 2005, **72**, 011602.
14. Wang, C. Y. and Beckermann, C., Equiaxed dendritic solidification with convection: Part I. Multiscale/multiphase modeling. *Metal. Mater. Trans. A*, 1996, **27**, 2754–2764.
15. Tong, X., Beckermann, C., Karma, A. and Li, Q., Phase-field simulations of dendritic crystal growth in a forced flow. *Phys. Rev. E*, 2001, **63**, 061601.
16. Pal, D., Bhattacharya, J., Dutta, P. and Chakraborty, S., An enthalpy model for simulation of dendritic growth. *Num. Heat Transf., Part B: Fundamentals*, 2006, **50**, 59–78.
17. Tan, L. and Zabaras, N., A level set simulation of dendritic solidification of multi-component alloys. *J. Comput. Phys.*, 2007, **221**, 9–40.
18. Hirt, C. W. and Nichols, B. D., Volume of fluid (VOF) method for the dynamics of free boundaries. *J. Comput. Phys.*, 1981, **39**, 201–225.
19. Sethian, J. A., Level Set Methods: Evolving Interfaces in Geometry, Fluid Mechanics, Computer Vision, and Materials Science, Cambridge University Press, Cambridge, UK, 1996.
20. Gerlach, D., Tomar, G., Biswas, G. and Durst, F., Comparison of volume-of-fluid methods for surface tension-dominant two-phase flows. *Int. J. Heat Mass Transf.*, 2006, **49**, 740–754.
21. Patankar, S. V., *Numerical Heat Transfer and Fluid Flow*, Taylor & Francis Group, New York, 1980.

Received 24 June 2013; accepted 28 June 2013